Computational and Structural Biotechnology Journal 16 (2018) 404–411

COMPUTATIONAL AND STRUCTURAL BIOTECHNOLOGY JOURNAL

journal homepage: www.elsevier.com/locate/csbj

In Vitro and *In Silico* Insights into sEH Inhibitors with Amide-Scaffold from the Leaves of *Capsicum chinense* Jacq.

Jang Hoon Kim *, Yeong Deuk Jo, Hyo-Young Kim, Bo-Ram Kim, Bomi Nam

Advanced Radiation Technology Institute, Korea Atomic Energy Research Institute, Jeongeup 56212, Republic of Korea

ARTICLE INFO

Article history:
Received 12 September 2018
Received in revised form 24 October 2018
Accepted 26 October 2018
Available online 31 October 2018

Keywords:
Capsicum chinense Jacq. cv. Habanero
Solanaceace
Amide-based inhibitors
Molecular docking
Molecular dynamics

ABSTRACT

Two compounds termed **1** and **2** were isolated from the leaves of *Capsicum chinense* using column chromatography. Their structures were identified as amide scaffolds by analyzing spectroscopic signals. Compounds **1** and **2** have been confirmed to be competitive soluble epoxide hydrolase (sEH) inhibitors that suppress the catalytic reaction of sEH in a dose-dependent manner *in vitro*. Molecular docking was used for analyzing two binding clusters of ligand and receptor. The results confirmed that the key amino acids interacting with the ligand were Asp335, Tyr383, and Gln384. On the basis of molecular dynamics, inhibitors **1** and **2** were noted to interact at a distance of 3.5 Å from Asp335, Tyr383, Leu408 and Tyr466, and Asp335, Tyr383, and Tyr466, respectively. These results highlight the potential of *N-trans*-coumaroyltyramine (**1**) and *N-trans*-feruloyltyramine (**2**) as sEH inhibitors.

1. Introduction

Capsicum chinense Jacq. cv. Habanero is an annual crop that belongs to the *Solanaceace* family and originates from the state of Amazonas, Brazil [1]. The plant grows to a height of 30–120 cm [1]. The fruits of *C. chinense* have globose, cylindrical, and elongated pods, with dimensions of 0.5, 2–5 × 1.5–3 (length x width), and 10 cm, respectively [1]. The fruits of this species are known to be one of the hottest peppers of the *Capsicum* species [2] and have been used in culinary spices and oriental medicines for treating headaches, night blindness, rheumatism, arthritis, and digestive diseases [2,3]. It has been reported that high-dose Habanero(0.08 g/kg dry matter/body weight)-treated rats didn't show pathological degeneration of the organs, such as stomach, duodenum, liver, and kidney tissues [4].

Capsaicin (*trans*-8-methyl-*N*-vanillylnon-6-enamide) and dihydrocapsaicin (8-methyl-*N*-vanillylnonanamide) are major volatile, hydrophobic, and colorless components of Capsicum fruits and provide heat to the peppers [3,5]. Two capsaicinoids have been shown to increase the expression of the tumor suppressor protein p54, which also plays a role in toxicity in lung epithelial cells [6]. Moreover, capsaicin is considered to improve gastric ulcers by suppressing acid secretion in the stomach [7].

Soluble epoxide hydrolase (sEH, E.C. 3.3.2.10) is a hydrolytic enzyme that converts epoxy-fatty acids to corresponding vicinal diols [8]. Epoxyeicosatrienoic acids (EETs) exist as four regioisomers (5,6-, 8,9-, 11,12-, and 14,15-EETs) that are derived from cytochrome *p*450 epoxygenase of arachidonic acid [9]. These EETs have various biological activities including vascular protection, anti-inflammatory, anti-arrhythmic, anti-patherosclerosis, and anti-migratory effects [10]. In contrast, dihydroxyeicosatrienoic acids (also derived via sEH activity) have less biological activity than EETs, and may exhibit increased toxicity [11]. Recent research has identified a role of sEH in the mitigation of hypertension, inflammation and cardiovascular disorders [12]. The urea-based sEH inhibitors, *trans*-4-[4-(3-adamantan-1-ylureido)cyclohexyloxy] benzoic acid (*t*-AUCB), *N*-(1-acetylpiperidin-4-yl)*N*′-(adamant-1-yl)urea (APAU), 1-adamantan-1-yl-3-(4-(3-morpholinopropoxy) cyclohexyl)urea (AMCU), and 12-(3-adamantan-1-yl-ureido)dodecanoic acid (AUDA) block the catalytic reaction of sEH [12,13]. However, their poor bioavailability owing to low solubility is considered an undesirable property [14]. In view of these factors, the development of novel and efficient inhibitors of sEH is clinically important.

* Corresponding author.
E-mail addresses: oasis5325@gmail.com, kjh53@kaeri.re.kr (J.H. Kim).

https://doi.org/10.1016/j.csbj.2018.10.017

In the present study, we identified phytochemicals present, *N-trans*-coumaroyltyramine (**1**) and *N-trans*-Feruloyltyramine (**2**), in *C. chinense* leaves. In previous study amide-based compounds were reported to be the potential inhibitor instead of urea based inhibitor on sEH [13]. Thus, the study was designed to determine that compounds derived from the natural product would likely bind to the active site of sEH. Our hypothesis that they will act similar to the urea type is proved by enzyme assay and kinetic studies, and molecular simulation.

2. Materials and Methods

2.1. General Experimental Procedures

Nuclear magnetic resonance (NMR) spectra were recorded using an ECA 500 MHz spectrometer (JEOL, Tokyo, Japan). Thin-layer chromatography analyses were performed using silica gel 60 F_{254} and RP-18 F_{254S} plates (both with a depth of 0.25 mm; Merck, Darmstadt, Germany). The compounds were visualized by dipping the plates into 10% (v/v) H_2SO_4 (Sigma-Aldrich, St. Louis, MO, US) and then heat-treated at 300 °C for 15 s. Silica gels (60, 70–230, or 230–400A American Standard Test Sieve Series mesh; Merck) and reversed-phase silica gels (ODS-A 12 nm S-150, S-75 μm; YMC Co., Dinslaken, Germany) were used for the column chromatography. Soluble Epoxide Hydrolase Kit (10009658) and PHOME (10009134) were purchased from Cayman (MI, US).

2.2. Plant Material

The leaves of *C. chinense* Jacq. cv. Habanero were cultivated and collected from experimental farm in Advanced Radiation Research Institute (Jeoungeup, Jeollabuk-do, Republic of Korea) in October 2017. The species was identified by Dr. Y.D. Jo of the Radiation Breeding Research Center, Korea Atomic Energy Research Institute. A voucher specimen has been deposited under accession number RBRC 002 at the herbarium of the Department of Natural Products, Radiation Breeding Research Center, Korea Atomic Energy Research Institute.

2.3. Extraction and Isolation

Habanero leaves (2 kg) underwent two extractions with 95% MeOH (36 L) at room temperature for seven days. The MeOH extract was concentrated under reduced pressure (2000 g) and suspended in distilled water. The suspension was partitioned by sequential extractions with *n*-hexane, chloroform, and ethyl acetate, and then BuOH. The chloroform faction (8 g) was subjected to silica gel column chromatography using acetone/*n*-hexane (0/1 → 1:1) to yield eight fractions (HC1–HC8). The HC4 fraction was chromatographed with C-18 column chromatography using MeOH/water (1/1 → 10:1) to obtain compound **1** (7 mg) and four further fractions (HC41–HC44). The HC43 fraction was purified with C-18 column chromatography using MeOH/water (1/1 → 9:1) to obtain compound **2** (5 mg).

2.4. sEH Enzymatic Assay

The sEH assay was performed with minor modifications in accordance with instructions present with the Cayman sEH kit. The sEH assay buffer was diluted ten-fold in HPLC water. For determining inhibitory activity, 90 μL of the diluted buffer was added to either 2.5 μL sEH (diluted fifty-fold in kit buffer) and 5 μL MeOH, or a solution of inhibitor dissolved in MeOH. Next, the substrate (PHOME) (2.5 μL) was added to each mixture, and sEH hydrolysis was allowed to proceed at 37 °C. The products were monitored at 330 nm excitation and 465 nm emission for approximately 40 min.

Inhibitory activity was calculated according to the following equations:

$$\text{Inhibitory activity rate } (\%) = [(\Delta C - \Delta I)/\Delta C] \times 100 \quad (1)$$

Where ΔC and ΔI are the intensity of control and inhibitor, respectively, after 40 min.

$$y = y_0 + (a \times x/b + x) \quad (2)$$

Where y_0 is minimum value of the *y*-axis, a is the difference between maximum and minimum values and b is the *x* value at 50% of the a value.

2.5. Molecular Docking

For docking the ligand into the receptor, two ligands of a 3D structure were constructed and minimized using Chem3D pro. The protein structure of the receptor was coded in 3ANS and downloaded from the RCSB protein data bank. Since only the A-chain of the enzyme was required, the B-chain was deleted. Water and 4-cyano-N-[(1*S*, 2*R*)-2-phenylcyclopropyl]- benzamide were then excluded from the A-chain. The revised A-chain was added to hydrogen using AutoDockTools, and was then subjected to Gasteiger charge. Flexible ligand was set up using the torsion tree with detecting torsion root and rotatable bonds. The grid box was set at a size of 40 × 50 × 50 at 0.375 Å for the docking of the ligand into the activity site. Molecular docking was achieved via the Lamarckian Genetic Algorithm with the maximum number of evaluations. Resulting values were calculated and represented using AutoDockTools, Chimera, and LigPlot.

2.6. Molecular Dynamics

Molecular dynamics (MD) was carried out using the GROMACS version 4.6.5. The 3D structure for MD simulation was extracted from the

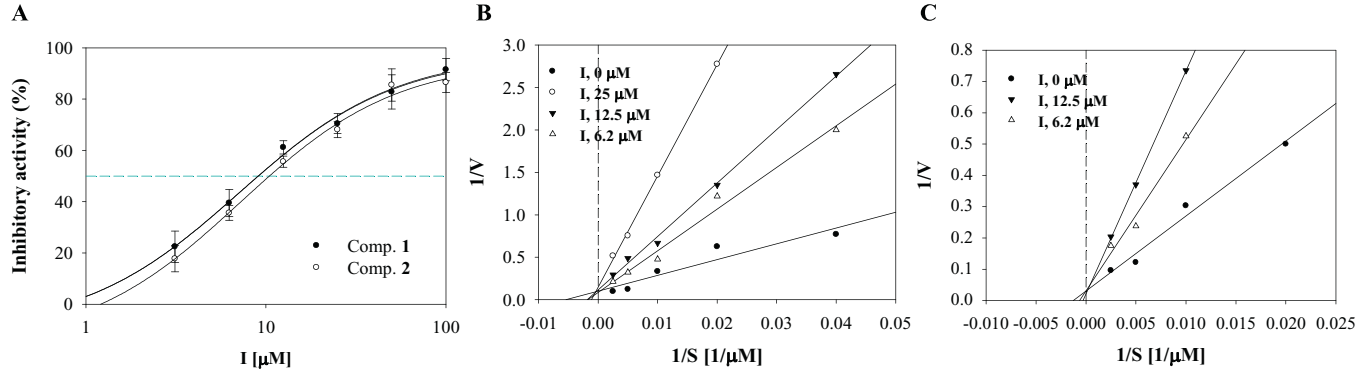

Fig. 1. Inhibitory activity (A) and Lineweaver-Burk plots (B and C) of compounds **1** and **2** on sEH.

Table 1
Inhibitory activity of compounds **1** and **2** on sEH.

	IC_{50} value[a,b]	Binding mode
1	9.0 ± 0.8	Competitive type
2	10.4 ± 1.1	Competitive type

[a] Tested three times
[b] Positive control was used as AUDA (IC_{50}: ~ 1 nM)

best docking pose; .gro and .itp file formats of structure ligand were built to the GlycoBioChem PRODRG2 server. A Gro file of the receptor, produced by pdb2gmx utility with GROMOS96 43a1 force field of Gromacs, was modified by appending the ligand information. The complexes of inhibitors **1** and **2** were eluted with cubic default size and cubic size of 8.5 × 8.5 × 8.5 by the addition of six Cl^- ions, respectively. Their energy minimization was stabilized up to 10.0 kJ/mol in steepest descent minimization. The receptor–ligand complex was sequentially subjected to NVT equilibration at 300 K, NPT with Particle Mesh Ewald for long-range electrostatics at 1 bar and MD simulation for 10 ns.

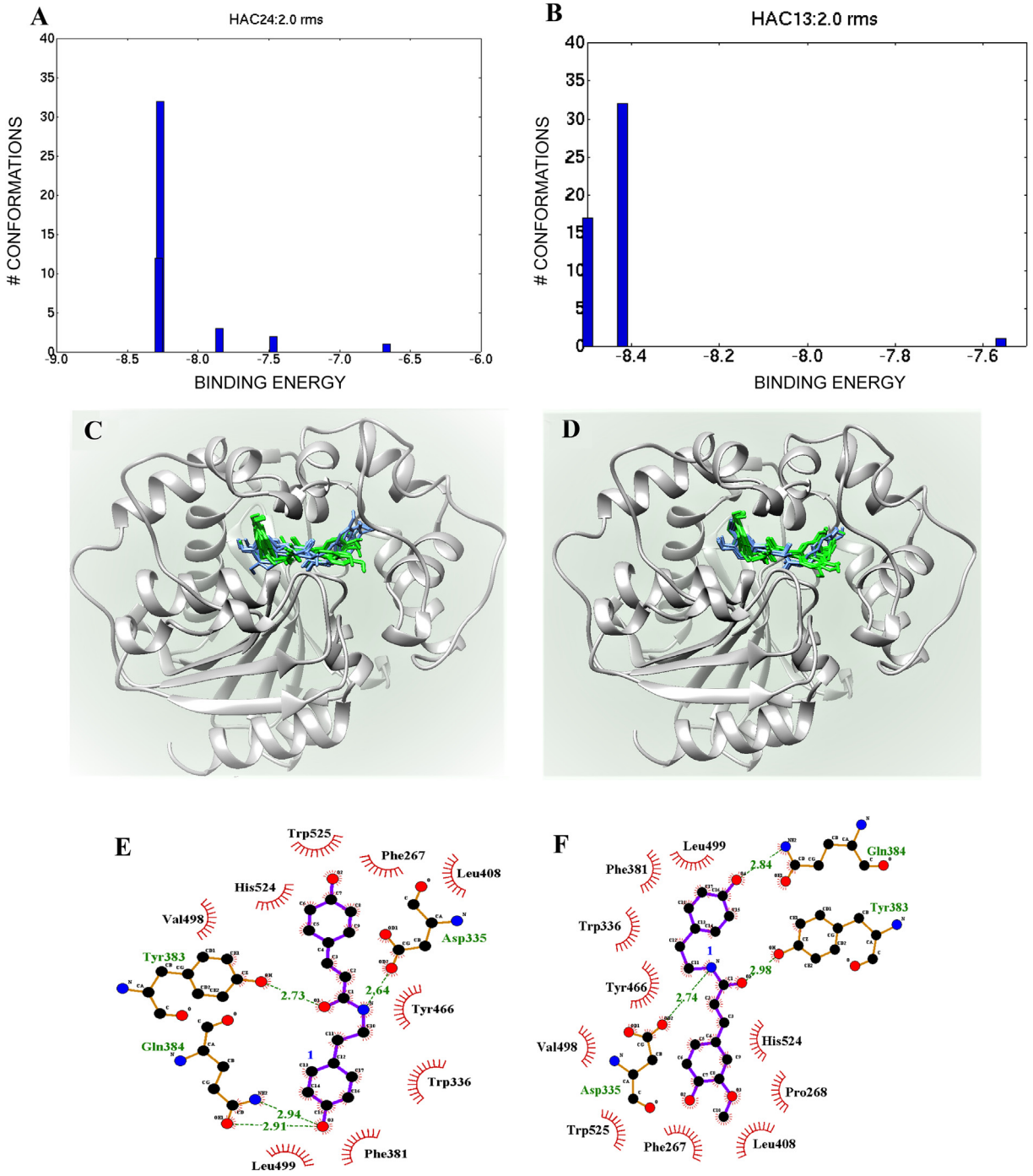

Fig. 2. Clustering (A and B) results and two cluster analysis (C and D; green: cluster 1, conflower blue: cluster 2) of Autodock docking score of compounds **1** and **2** in sEH. Best pose (E and F) of inhibitors (**1** and **2**) docked into catalytic site of enzyme.

Table 2
Binding cluster and hydrogen bonds analysis of inhibitor with sEH.

Autodock score ranks	Compound **1**		Compound **2**	
	Cluster 1	Cluster 2	Cluster 1	Cluster 2
1	Asp335,Tyr383, Gln384	Asp335,Tyr383,	Asp335, Tyr383, Gln384	Asp335, Tyr383
2	Asp335,Tyr383, Gln384	Asp335,	Asp335, Tyr383, Gln384	Asp335, Tyr383
3	Asp335,Tyr383, Gln384	Asp335,	Asp335, Tyr383, Gln384	Asp335, Tyr383
4	Asp335,Tyr383, Gln384	Asp335,	Asp335, Tyr383, Gln384	Asp335, Tyr383
5	Tyr383, Gln384	Asp335,Tyr383,	Asp335, Tyr383, Gln384	Asp335, Tyr383
6	Tyr383, Gln384	Asp335,Tyr383,	Asp335, Tyr383, Gln384	Asp335, Tyr383
7	Gln384	Asp335,Tyr383,	Gln384	Asp335, Tyr383
8	Asp335,Gln384	Asp335,Tyr383,	Tyr383,	Asp335
9	Asp335,Tyr383, Gln384	Asp335, Tyr466, Met339	Tyr383, Gln384	Asp335, Tyr383
10	Tyr383	Asp335	Tyr383,	Asp335, Tyr383

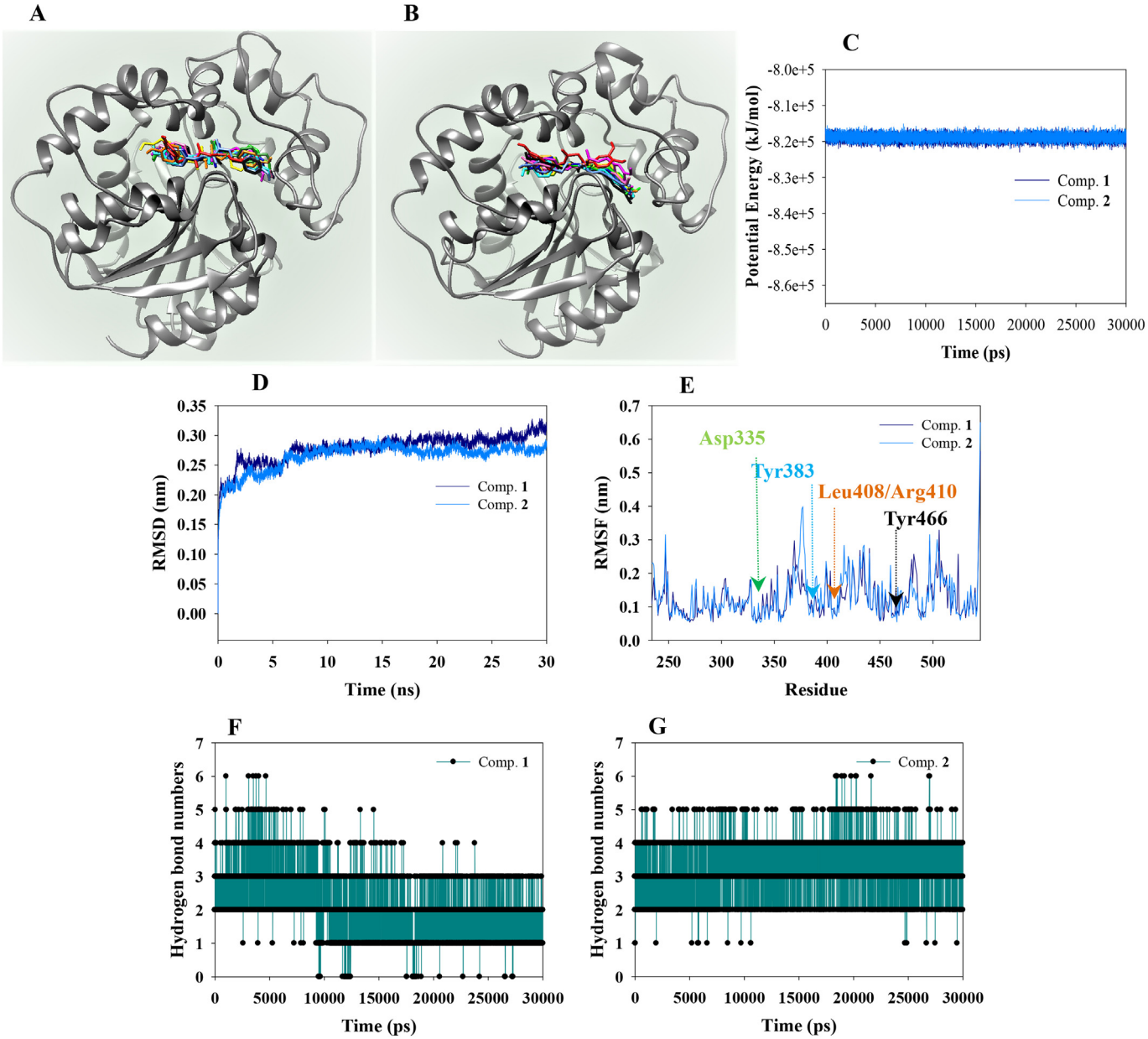

Fig. 3. The superpositions of inhibitor (**1** and **2**) into sEH for the simulation time (red: 0, orange: 3, yellow: 6, green: 9, forest green: 12, cyan: 15, blue: 18, conflower blue: 21, hot pink: 24, magenta: 27, and black: 30 ns). The potential energy (C), RMSD (D), RMSF (E), and hydrogen bond numbers (F and G) of **1** and **2** with sEH.

Table 3
Hydrogen bonds analysis of inhibitor with sEH at 3 ns intervals for the simulation times.

Time (ns)	Compound **1**	Compound **2**
	Reidue (Å)	Reidue (Å)
0	Tyr383(2.62), Gln384(2.82)	Asp335(3.04), Tyr383(2.53)
3	Tyr383(2.46), Asp335(3.24)	Asp335(2.91), Tyr383(2.53), Tyr466(2.69)
6	Asp335(3.03), Tyr383(2.40),. Leu408(2.92)	Asp335(3.08), Tyr383(2.61), Tyr466(2.60)
9	Tyr383(2.51), Leu408(3.06), Tyr466(2.52)	Asp335(3.25), Arg410(3.20), Tyr383 (2.65), Tyr446(2.82)
12	Tyr383(2.45), Asp335(2.89), Leu408(3.15)	Asp335(3.15), Tyr383(2.52), Tyr446(2.61)
15	Tyr383(2.53), Leu408(3.01)	Arg410(2.94), Tyr383(2.55), Tyr446(2.83)
18	Tyr383(2.54), Leu408(3.09), Tyr466(3.34)	Asp335(3.22),Tyr383(2.58), Arg410 (3.22), Tyr446(2.55), Trp525(2.83)
21	Asp335(3.13), Tyr383(2.64), Leu408(2.92)	Asp335(3.10), Tyr383(2.46), Tyr446 (2.71), Arg410(3.27)
24	Asp335(2.99), Tyr383(2.63)	Asp335(3.18), Tyr446(2.77)
27	Asp335(3.02), Tyr383(2.66)	Asp335(3.10), Tyr383(2.46), Tyr446 (2.71), Arg410(3.27)
30	Tyr383(2.56), Tyr466(2.90)	Tyr383(2.76), Arg410(3.15), Tyr446(2.78)

2.7. Statistical Analysis

All data in the presence of inhibitors wereperformed at least three independent experiments carried out in triplicate, and the results were showed up as the means±standard error of the mean (SEM). The results were subjected to analysis using Sigma Plot (SPP Inc., Chicago, IL, USA). Statistical significance is indicated as determined by one-way ANOVA followed by Dunnett's multiple comparison test $P < 0.05$, using GraphPad Prism 6 (GraphPad Softweare Inc., San Diego, CA, USA).

3. Results and Discussion

3.1. Isolation and Identification

The MeOH extracts of Habanero leaves were sequentially divided in *n*-hexane, chloroform, ethyl acetate, butanol, and water, respectively. Of these, the chloroform fraction was purified using silica gel and C-18 column chromatographies to yield the two compounds **1** and **2**. The chemical structures of *N-trans*-coumaroyltyramine (**1**) [15] and *N-trans*-feruloyltyramine (**2**) [16] were elucidated by analyzing the signals of ESI-Ms and ^{1}H NMR spectrophotometers and by comparison with reported data.

3.2. sEH Inhibitory Assay

Compounds **1** and **2** were evaluated for sEH inhibition on the basis of the level of fluorescent 6-methoxy-2-naphthaldehyde formed via sEH-induced catalytic reaction with (3-phenyl-oxiranyl)-acetic acid cyano-(6-methoxy-naphthalen-2-ly)-methyl ester [10]. The product was quantified in the presence or absence of the inhibitor using a fluorescence photometer with excitation and emission wavelengths of 330 and 465 nm, respectively [10]. For evaluating the inhibitory activity of compounds **1** and **2** on sEH, assays were performed using a variety of concentrations ranging from 100 to 6.25 μM. Inhibitory activities were calculated as a percentage using Eq. 1. The rate of inhibition was noted to decrease in a dose-dependent manner on the basis of inhibitor concentration. The calculated dots in Fig. 1A were fitted by Eq. 2 for calculating IC_{50} values. Compounds **1** and **2** were noted to have IC_{50} values of 9.0 ± 0.8 and 10.4 ± 1.1 μM, respectively (Table 1).

The urea-type derivatives *t*-AUCB, APAU, and AUDA have been developed as candidates for the treatment of cardiovascular diseases [12,13,17]. They exhibit inhibition of this catalytic reaction by binding to the active site of sEH [17]. However, low solubility limits their potential use in medicine [17]. Several studies have been conducted for identification of a novel scaffold that overcomes this solubility issue [10,11,13,14]. Subsequently, *N*-(3,3-diphenyl-propyl)-nicotinamide and *N*-[3,3-bis-(4-fluorophenyl)-propyl]-nicotinamide were identified as amide-based scaffolds. They both showed potential as sEH inhibitors at IC_{50} values of <10 nM in both humans and rats [13]. These observations confirmed that compounds **1** and **2** can be used for determining the inhibitory activity of sEH. In the present study, different values of initial rates of inhibition were observed according to the substrate concentration used (ranging from 1.56 to 25 μM). Fig. 1B and C show two concentrations with similar V_{max} and different K_m values in Lineweaver–Burk plots. On the basis of these results, the inhibitors

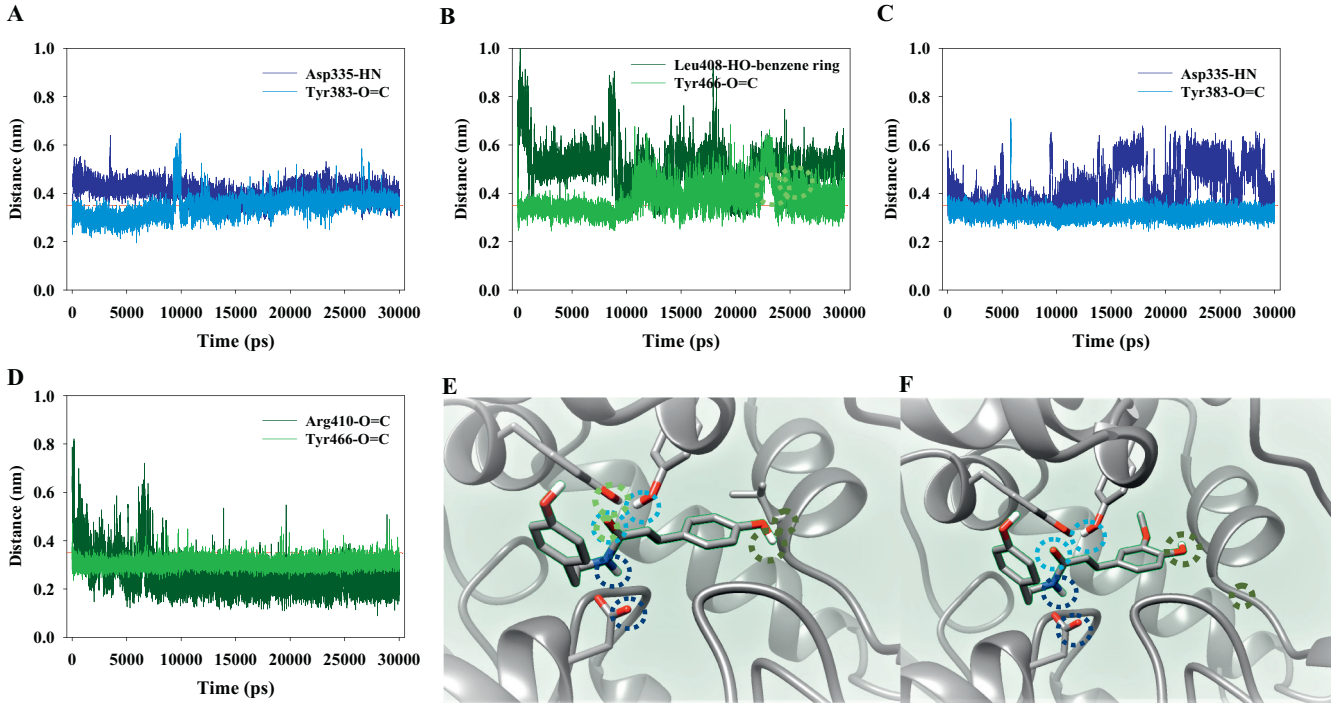

Fig. 4. The distance (A-B) of respective compounds **1** and **2** with key amino acids (E-F).

showed familiarity with the active binding site of sEH (Table 1). X-ray crystallography of sEH with urea-based inhibitors revealed the interaction at the catalytic site of the enzyme [13]. Additionally, an amide moiety showing a chemical structure similar to that of urea-based inhibitors was found to be located at the same site.

3.3. Molecular Docking

Inhibitors **1** and **2** dock into the catalytic region of sEH. Molecular docking was performed to shed light on the sEH inhibitor interaction using Autodock version 4.2. Molecular simulation was performed to construct a grid containing the full active site for accurate and effective investigation. For delicate search of receptor and ligand, the molecular simulation was subjected to docking over 25 million times. The top 50 Autodock scores were extracted for an accurate simulation analysis. The selected 50 best poses for inhibitors **1** and **2** were divided into two clusters (Fig. 2A and B). Two ligand phenols of the lower cluster were directed outward from the center of sEH (Fig. 2C and D). In the other cluster, aromatic rings were oriented in the direction of the center (Fig. 2C and D). Lower autodock score clusters were often composed of a main hydrogen bond with Asp335, Tyr383 and Gln384 (Table 2). The others usually comprised hydrogen bonds with Asp335 and Tyr383 (Table 2). The lowest autodock score of −8.28 kcal/mol for compound **1** related to hydrogen bonds with Asp335 (2.64 Å), Tyr383 (2.73 Å), and Gln384 (2.91 and 2.94 Å) (Fig. 2E). Moreover, amide and phenol groups in compound **2** interacted with Asp335 (2.64 Å), Tyr383 (2.73 Å) and Gln384 (2.91 and 2.94 Å) at a rate of −8.28 kcal/mol, respectively (Fig. 2F).

sEH converts the epoxide of EET to diol through a catalytic triad comprising Asp333, Asp495, and His523 [18]. The substrate interacts with the triad to allow binding to the enzyme. Urea-based inhibitors also increase the stability of the receptor by maintaining hydrogen bonds with Asp333, Tyr381 and Tyr465 [19]. Additionally, the amide-based inhibitors *N*-(3,3-diphenyl-propyl)-nicotinamide and pyridine-3-sulfonic acid 3,3-(diphenylpropyl)-amide, enhance enzyme binding through the interaction with these three residues [13]. In this study,

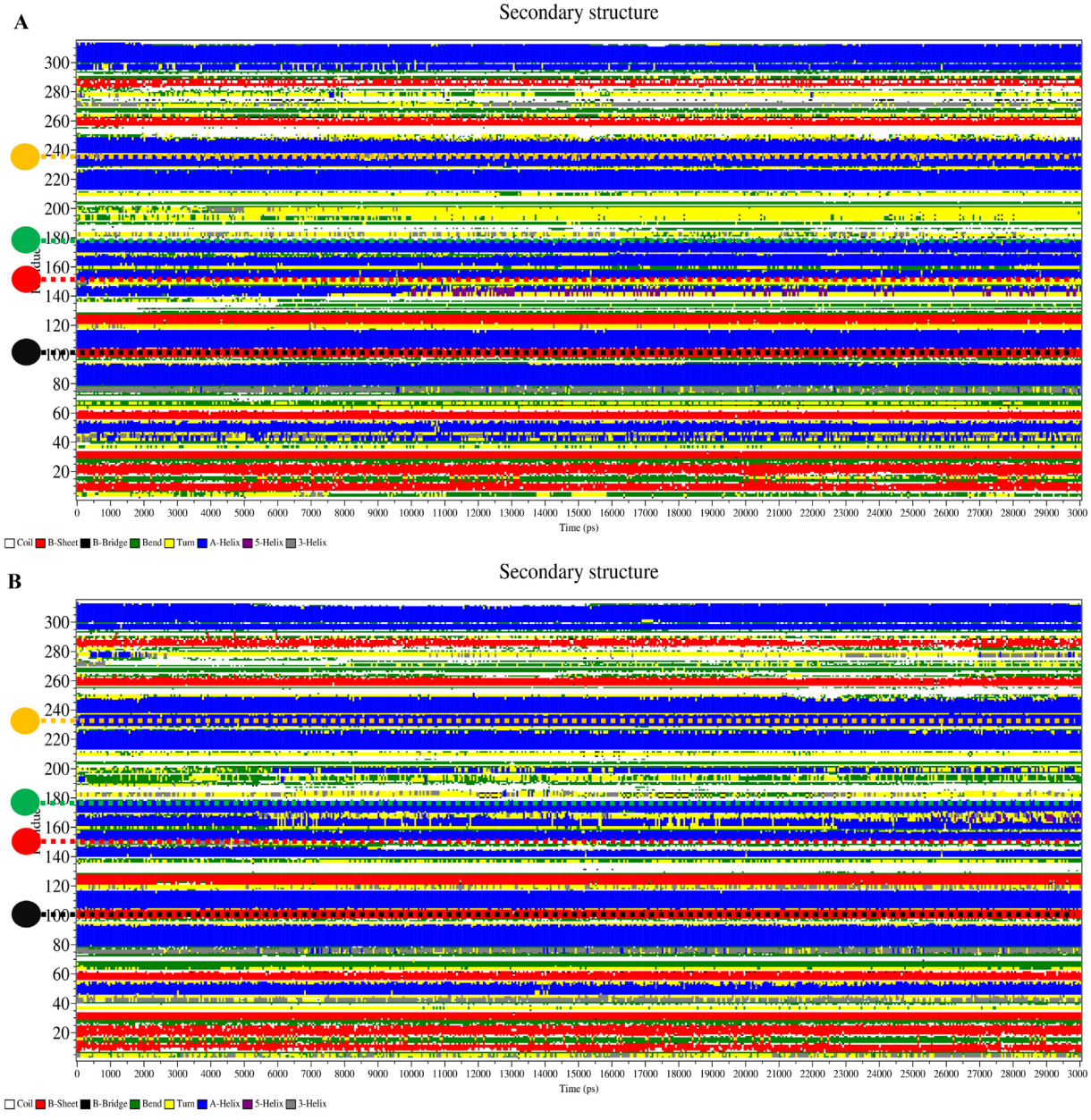

Fig. 5. Secondary structure changes in protein interacted with compounds **1** (A) and **2** (B) (black dot line: Asp335, led dot line: Tyr383, green dot line: Leu408/Arg410, and orange dot line: Tyr466).

the inhibitors **1** and **2** showed similar levels of interaction, although their phenol group was linked to the hydrogen bond of Gln384 instead of Tyr465. These observations provide further information on the receptor with an amide-based moiety, and facilitate the development of a novel sEH inhibitor. The structures of the compounds showed differences in the presence or absence of methoxyl groups. The two bound the catalytic sites and their bioactivity was very similar. It was confirmed that they didn't participate in hydrogen bonding at the part where they differ from each other. This result fully explains why the two compounds have similar activity values.

3.4. Molecular Dynamics

MD is a state-of-the-art technique that allows movement of rigid receptor and ligand complexes. On the basis of the mobility of the complex, MD can be considered as a useful tool for the development of the inhibitors as drugs [20]. This study was performed using Gromacs version 4.6.5 and PRODRG server. Using molecular docking, key amino acids (Asp335, Tyr383, and Gln384) were identified owing to the docking of flexible ligand into rigid receptor. MD analysis can support these docking results through the fluidity of their complexes, or identify new key interactions [21].

According to the MD simulation results, ligands **1** and **2** showed a very high level of free flowability in the catalyst site with potential energy values of -8.1×10^5 kJ/mol (Figs. 3A–C). The root-mean-square deviation (RMSD) of inhibitors **1** and **2** showed a similar pattern and achieved maximum equilibrium by 0.25–0.30 nm, within 2 ns of the MD simulation (Fig. 3D). The root-mean-square fluctuation (RMSF) utility of Gromacs was used to analyze the respective mobility of the amino acids, which showed flexibilities of under 0.3 nm. However, Asp335, Tyr383, Leu408, and Tyr466, all of which interact with the ligands, were not observed to move >0.08 nm (Fig. 3E). Of note, inhibitor **1** maintained an average of 1–3 hydrogen bonds with the key amino acids (Asp335, Tyr383, Leu408, Tyr466) of the sEH catalyst site (Fig. 3F and Table 3). Moreover, inhibitor **2** is mainly composed of 2–4 hydrogen bonds with Asp335, Asp383, Tyr466, and Arg410 residues (Fig. 3G and Table 3).

Key amino acids were calculated the distance of respective ligands (**1** and **2**) for simulation times by g_dist utility for detailed interaction of them. Inhibitor **1** maintains a consistent distance of 3.5 Å from the amide and hydroxyl groups of respective Tyr383, Asp335 and Tyr466 residues. Additionally, Leu408 was sometimes located at 3.5 Å from the ligand (Fig. 4A, B and E). Inhibitor **2** docked in a similar pose to **1** at a distance approximately 3.5 Å from Asp335, Tyr383, Tyr466, and Arg410 (Fig. 4C, D and F). MD analysis not only supported the molecular docking results, but also revealed new key amino acids such as Leu408 and Arg410 that bind with the ligand. Furthermore, this study used the Dictionary of Secondary Structure of Proteins (DSSP) to elucidate the change of secondary structure caused by inhibitors **1** and **2**. Fig. 5A and B show β-Sheet and α-Helix secondary structures including Asp335, Leu408/Arg410 and Tyr466 at the start of the MD procedure. Changes in their secondary structure were not observed even after simulation of 30 ns. However, it was possible to confirm that the 3-Helix of Tyr383 shows a change in structure to a turn type (Fig. 5A and B). In the sEH inhibitors **1** complex, the 3-Helix of Tyr383 changed to a turn type mainly during the simulation time; Tyr383 was confirmed to participate in hydrogen bonding with the ligand (Fig. 5A).

Also in the MD experiment, the two compounds had similar parameter values. They were found to have hydrogen bonds with respective Leu408 and Arg410 amino acids. sEH docked by **1** was confirmed their secondary structure of around Tyr383 made a shape as turn type for 30 ns. Whereas, the complex of receptor with **2** mainly ketp α-Helix secondary structure. As mentioned above, the difference between the two seemed to have no significant effect on their overall similarity. These facts have been demonstrated *in vitro*, and *in silico* virtually suggested the binding pattern and key amino acids between the ligand and receptor.

4. Conclusion

N-trans-coumaroyltyramine(**1**) and *N-trans*-feruloyltyramine(**2**) were isolated from the extract of Habanero leaves using silica gel and C-18 column chromatography. These compounds exhibited an inhibitory activity on sEH, with IC_{50} values of approximately 10 μM. The Lineweaver–Burk plots indicate that they competitively bind to the catalyst site of the enzyme. In an analysis of the top 50 molecular docking results, the two inhibitors were associated with several amino acids of sEH in the formation of two similar clusters. The key amino acids that interact with inhibitors **1** and **2** are Asp335, Tyr383, and Gln384. MD analysis determined the number of hydrogen bonds between ligand and receptor, the mobility of key residues, and secondary structure changes. These results suggest that Tyr466 may be more important than Gln384 in ligand binding. In summary, this study has identified two amide derivatives extracted from *C. chinense* leaves that act as natural inhibitors of sEH. The interactions of Asp335, Tyr383, and Tyr466 in the complex should be considered during the development of novel amide sEH inhibitors.

Conflicts of Interest

The authors declare no conflict of interest.

Acknowledgements

This research was supported by Radiation Technology R&D program (No.2017M2A2A6A05018541) through the National Research Foundation of Korea (NRF) funded by the Ministry of Science, ICT & future Planning.

References

[1] Lim TK. Edible medicinal and non-medicinal plants. Fruits. Springer; 2013. p. 205–12.
[2] M S, Chhapekar SS, Ahmad I, Abraham SK, Ramchiary N. Analysis of bioactive components in ghost chili (Capsicum chinense) for antioxidant, genotoxic, and apoptotic effects in mice. Drug Chem Toxicol Jul 22, 2018:1–10.
[3] Davis CB, Markey CE, Busch BA, Busch KW. Determination of capsaicinoids in Habanero peppers by chemometric analysis of UV spectral data. J Agric Food Chem 2017; 55:5925–33.
[4] golynski M, balicki I, Lutnicki K, Smiech A, Adamek L, Szczepanik M, et al. Systemic and local effects of intragastric administration of the habanero fruit (Capsicum Chinense Jacquin C.V.) in rats. J Physiol Pharmacol 2015;66:259–65.
[5] Gayathri N, Gopalakrishnan M, Sekar T. Phytochemical screening and antimicrobial activity of *Capsicum chinense* Jacq. Int J Adv Pharm 2016;5:12–20.
[6] Halme M, Pesonen M, Salo H, Söderström M, Pasanen M, Vähäkangas K, et al. Comparison of *in vitro* metabolism and cytotoxicity of capsaicin and dihydrocapsaicin. J Chromatogr B 2016;1009–1010:17–24.
[7] Das SK, Teja C, Duary B, Agrawal PK, Bhattacharya SS. Impact of nutrient management, soil type and location on the accumulation of capsaicin in *Capsicum chinense* (Jacq.): one of the hottest chili in the world. Sci Hortic 2016;213:354–66.
[8] Burmistrov V, Morisseau C, Danilov D, Harris TR, Dalinger I, Vatsadze I, et al. 1,3-disubstituted and 1,3,3-trisubstituted adamantly-ureas with isoxazole as soluble epoxide hydrolase inhibitors. Bioorg Med Chem Lett 2015;25:5514–9.
[9] Batchu SN, Lee SB, Samokhvalov V, Chaudhary KR, El-Sikhry H, Wdldon SM, et al. Novel soluble epoxide hydrolase inhibitor protects mitochondrial function following stress. Can J Physiol Pharmacol 2012;90:811–23.
[10] Xu M, Hao H, Jiang L, Long F, Wei Y, Ji H, et al. *In vitro* inhibitory effects of ethanol extract of Danshen (*Salvia miltiorrhiza*) and its components on the catalytic activity of soluble epoxide hydrolase. Phytomedicine 2015;22:444–51.
[11] Pecic S, Zeki AA, Xum X, Jin GY, Zhang S, Kodani S, et al. Novel peperidine-derived amide sEH inhibitors as mediators of lipid metabolism with improved stability. Prostaglandins Other Lipid Mediat 2018;136:90–5.
[12] Huang S-X, Cao B, Morisseau C, Jin Y, Hammock BD, Long Y-Q. Structure-based optimization of the piperazino-containing 1,3-disubstituted ureas affording subnanomolar inhibitors of soluble epoxide hydorlase. Med Chem Commun 2012(3): 379–84.
[13] Eldrup AB, Soleymanzadeh F, Taylor SJ, Muegge I, Farrow NF, Joseph D, et al. Structure-based optimization of arylamides as inhibitor of soluble epoxide hydrolase. J Med Chem 2009;52:5880–95.

[14] Kim I-H, Park Y-K, Nishiwaki H, Hammock BD, Nishi K. Structure-activity relationships of amide-phosphonate derivatives as inhibitors of the human soluble epoxide hydrolase. Bioorg Med Chem 2015;23:7199–210.
[15] Kamdem RST, Wafo P, Dawe A, Nganteng DND, Ogechukwu UB, Rasheed S, et al. Bioactive chemical constituents of *Duboscia macrocarpa* Bocq., and X-ray diffraction study of 11b, 12b-epoxyfriedours-14-en-3a-ol. Fitoterapia 2018;125:65–71.
[16] Hwang JT, Kim Y, Jang H-J, Oh H-M, Lim C-H, Lee SW, et al. Study of the UV light conversion of Feruloyl amides from *Portulaca oleracea* and their inhibitory effect on IL-6-induced STAT3 Activation. Molecules 2016;21:865.
[17] Imig JD, Hammock BD. Soluble epoxide hydrolase as a therapeutic target for cardiovascular diseases. Nat Rev Drug Discov 2009;8:794–805.
[18] Kramer J, Proschak E. Phosphatase activity of soluble epoxide hydrolase. Prostaglandins & other lipid mediators. Prostaqlandins Other Lipid Mediat 2017;133:88–92.
[19] Lukin A, Kramer J, Hartmann M, Weizel L, Hernandez-Olmos V, Falahati K, et al. Discovery of polar spirocyclic orally bioavailable urea inhibitors of souble epoxide hydrolase. Bioorg Chem 2018;80:655–67.
[20] Cheng P, Li J, Wang J, Zhang X, Zhai H. Investigation of FAK inhibitors: a combination of 3D-QSAR, docking and molecular dynamics simulations studies. J Biomol Struct Dyn 2018;36:1529–49.
[21] Lv M, Ma S, Tian Y, Zhang X, Zhai H, Lv W. Structural insights into flavones as protein kinase CK2 inhibitors derived from a combined computational study. RSC Adv 2015;5:462–76.